Surface & Coatings Technology 218 (2013) 142–151

Contents lists available at SciVerse ScienceDirect

Surface & Coatings Technology

journal homepage: www.elsevier.com/locate/surfcoat

Stability of expanded austenite, generated by ion carburizing and ion nitriding of AISI 316L SS, under high temperature and high energy pulsed ion beam irradiation

J. García Molleja [a,*], M. Milanese [b], M. Piccoli [c], R. Moroso [b], J. Niedbalski [b], L. Nosei [d], J. Bürgi [a], E. Bemporad [c], J. Feugeas [a]

[a] Instituto de Física Rosario (CONICET-UNR), Bvrd. 27 de Febrero 210 Bis, S2000EZP Rosario, Argentina
[b] Instituto de Física Arroyo Seco (CONICET-UNCPBA), Pinto 399, B7000GHG Tandil, Argentina
[c] Dipartimento di Ingegneria Meccanica e Industriale (Università Roma Tre), Via della Vasca Navale 79, 00146 Rome, Italy
[d] Instituto de Mecánica Aplicada y Estructuras (FCEIyA-UNR), Berutti y Riobamba, S2000EKD Rosario, Argentina

ARTICLE INFO

Article history:
Received 29 June 2012
Accepted in revised form 19 December 2012
Available online 6 January 2013

Keywords:
Ion carburizing
Expanded austenite
Plasma focus
Crystalline stability

ABSTRACT

Expanded austenite can be generated on austenitic stainless steels either by ion carburizing or ion nitriding. In both cases the resulting fcc crystal structure, supersaturated with nitrogen or carbon, is strongly hardened with improved wear-resistance, while maintaining the original resistance to corrosion. In this work, we have studied the stability of expanded austenite, generated by ion nitriding and ion carburizing on AISI 316L SS with N and C, under: a—high temperature (225 °C – 504 °C), and b—under irradiation with high energy (30 keV – 500 keV), high fluence (~10^{15} cm^{-2}), short duration (~400 ns) light (deuterium and helium) ion beams. It was found that expanded austenite is stable below 325 °C. Between 325 °C and 504 °C expanded austenite lattice parameter presents gradual reduction with increasing temperature. We observed microstructural changes related only to the temperature treatment. We did not observe any microstructure change due to the duration of the heat treatment. Over 504 °C, the lattice parameter returns to the material's austenite original parameter. On the other hand, when irradiated with pulsed ion beams, a gradual reduction of the lattice parameter corresponding to the expanded austenite with the number of pulses was observed. This behavior can be explained through the thermal shock induced on the surface by each beam, consisting in fast heating followed by fast cooling that induces the gradual exo-diffusion of N (or C). Nevertheless, after 20 ion pulses, a final lattice parameter slightly higher than the corresponding to the original austenite was found as stable limit. This residual expansion can be attributed to partial amorphization of the first few micrometers that induces stresses on the crystals of austenite which are closer to the surface layers.

1. Introduction

Austenitic stainless steels, like AISI 316L grade, have been applied fluently for industrial purposes. Principal applications are: tools and home cutlery, tanks, pipes in food industry and tools and implements in surgery, among others. These uses are motivated by the excellent properties that austenitic stainless steels have, like good corrosion resistance to chloride pitting, great hygiene-cleanliness factor, of easy transformation, good welding properties, no hardening by heat treatment, and resistant to high and low temperatures. Nevertheless, they do not have important mechanical properties principally showing low hardness and poor wear resistance. More recently, a method has been found for wear and hardness improvements by the development of expanded austenite (called EA, *S*, *m*, *S′*, *ε′* or *γ* phase) on surface, without the loss of resistance to corrosion [1–4]. This phase is the result of nitrogen or carbon atoms entering in an fcc crystalline structure until the colossal supersaturation is reached [5] when a high number of these atoms occupy the fcc interstitial sites, presumably the octahedral ones. The consequence is the deformation of crystalline structure by compressive strains and high density of stacking faults that induce the lattice parameter growth. Other authors [6,7] support that EA is not an fcc structure but an fct, bct or trigonal structure. Nevertheless, in reference [8] it has been shown that EA has an fcc structure when strains are suppressed.

Ion nitriding [9] and carburizing [10] are techniques based on surface modification that are applied to obtain EA through nitrogen or carbon diffusion in the lattice of austenite, respectively. Indeed, low pressure cold plasma allows forming a thick EA case without nitride or carbide precipitation, conferring hardness and wear resistances to surfaces of austenitic stainless steels, well above the original material.

In this paper, we have studied the stability of the EA, developed either by ion nitriding and ion carburizing, under high temperature and by the incidence of high energy, high fluence rate, short duration pulsed ion beams generated in plasma focus discharges.

* Corresponding author. Tel.: +54 341 4853222; fax: +54 341 4821772.
E-mail address: garciamolleja@ifir-conicet.gov.ar (J. García Molleja).

0257-8972/$ – see front matter © 2013 Elsevier B.V. All rights reserved.
http://dx.doi.org/10.1016/j.surfcoat.2012.12.043

It is necessary to consider that the effect of ion beam irradiation on materials has importance on nuclear technology itself. In fact, super-austenitic steels (D9 type SS for example) are used for fuel clad and fuel wrapper in fast breeder reactors, in which the material is strongly irradiated by fast neutrons from nuclear reactions. Neutron irradiation reduces the duration of structural components mainly by changes on their dimensions. Such effect is induced by void swelling development in the bulk. For research purposes, and to accelerate such a void swelling effect, neutron fluxes can be replaced by energetic ion beams [11,12].

In addition, similar problems can be found in nuclear fusion technology. Whatever the concept for fusion reactors could be, i.e. magnetic fusion energy (MFE) [13] or inertial fusion energy (IFE) [14,15], there is a common need for future power-plants based on the extraction, through the wall structure, of the energy originated by the nuclear fusion reaction in the reactor core. Indeed, the first wall is the layer that will receive primary radiation consisting, for D–T nuclear fusion cycle, in energetic photons, 14.1 MeV neutrons and ions (mainly deuterium and helium). In spite of MFE consisting of a continuous radiating flux, other additional effects have to be considered in IFE. IFE fusion reaction takes place in very short times (several nanoseconds) generating an extremely high flux of radiation that will induce high temperatures and strong mechanical shocks on the surface of the first wall. This effect will last a short time and will be produced several times per second as established by requirements for concepts under research. Considering that steels (low activation steels) are potential candidates for the construction of the first wall, high power ion beam fluxes like the ones used in this paper can be of interest for material testing.

2. Experimental

2.1. Ion carburizing and nitriding

A new 5.1 l of capacity reactor made of AISI 304L SS (Fig. 1) was employed for ion carburizing and ion nitriding samples. The cathode was made of superposed AISI 304L SS 6 mm thick and 122.8 mm diameter disks (Fig. 2). The lower disk is directly connected to the power supply and the upper one, which has nine holes of 20.5 mm of diameter symmetrically distributed, serving as sample's lodging to avoid the sharp edge effect of electric discharges during the process [16,17]. The gas mixture belongs to cylinders of high purity (argon: 4.5, hydrogen: 4.8, methane: 4.5, nitrogen: 5.0), which are introduced into the chamber through a Pyrex glass pipe at 9 mm above cathode.

Base pressure was ~10^{-3} mbar, and cleaning plasma of hydrogen was systematically used during 15 min to eliminate mainly the remaining water adsorbed on samples and internal walls of chamber. Then, a heating process follows consisting in a plasma generation of 80% of H_2 and 20% of Ar gas mixture until samples reach the working temperature, i.e. 400 °C. Once the heating process is finished, the atmosphere is changed to the processing one which is 50% Ar–45% H_2–5% CH_4 for carburizing, and by 80% H_2–20% N_2 for nitriding, at 5 mbar in both cases. The time processing was 80 min in all cases.

2.2. Pulsed ion beam

Irradiation effect on EA has been performed by the ion beams accelerated in dense plasma focus (DPF) discharges [18,19]. The DPF used was a 2 kJ Mather type 40 mm free length electrodes, consisting in a coaxial pipe configuration with a 40 mm diameter anode, 15 mm long Pyrex insulator and an external electrode (cathode) made up of 12 bars disposed on a 100 mm diameter circumference. This device is basically a Z-pinch experiment [20] consisting in a fast discharge in a 1.6 mbar pure gas pressure between electrodes generating in the end a high density plasma column in front of the anode and along the symmetry axis of the coaxial electrode system [21]. It is in this stage of the process in which ions and electron beams are accelerated to

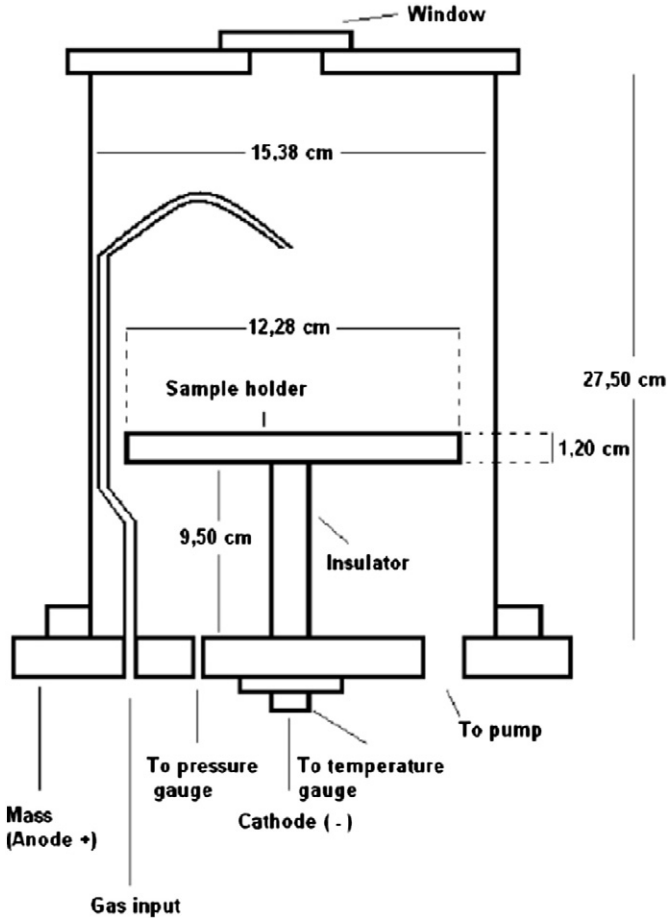

Fig. 1. Sketch of the vacuum chamber.

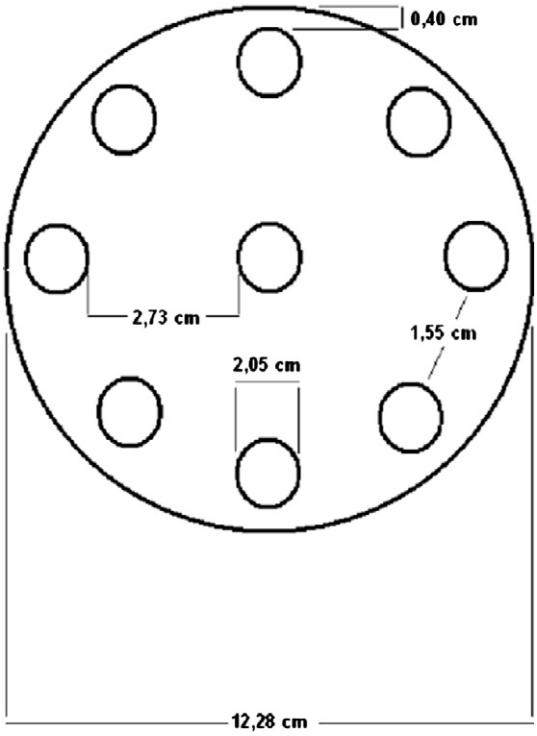

Fig. 2. Design of the sample holder.

the front and to the back, respectively [22–24]. The nature of the accelerated ions depends on the nature of the filling gas which in our case was deuterium and helium. The energy of the ions in the beams has a continuous spectrum ranging between 30 keV and 500 keV.

In our experiments samples are located at 82 mm from the front of the anode.

Under such experimental configuration surfaces receive an ion beam pulse with a fluence of ~10^{15} cm^{-2} with pulse duration of ~400 ns. This high resulting fluence rate induces a fast heating effect on surface layers due to the fast energy release of ions. Taking into account the ion range for the maximum ion energy available on beams (~500 keV), which is ~2.43 μm for deuterons on Fe, the energy will be released within a thin surface layer of equivalent thickness. This energy transfer process will result in a fast temperature increase during ~400 ns up to thousands of degrees, followed by fast cooling by thermal conduction to the sample bulk. This fast cooling process returns sample surface to room temperature in tens of microseconds. This process has been studied elsewhere [25,26] and can be considered as an ion beam induced *thermal shock*.

Pulses of ion beam can be produced in Plasma Focus experiments several times per second allowing sequences that can be considered as an approach to the one produced in laser induced IFE experiments. To study the accumulative effects, we have experimented with pulse sequences of 1, 5, 10 and 20 [27], with a frequency of ~1 Hz. Considering the fast cooling process (tens of microseconds) we can ensure that every ion beam pulse in the sequence will reach the sample surface at room temperature.

2.3. Heat treatment

Ion nitride and ion carburized samples were heat treated to study the variation of lattice parameters of the EA developed. Heat treatments were realized in a VEFBEN 15A–380 V furnace at normal atmosphere. Times employed were 20, 40 and 60 h at different temperatures: 225 °C, 325 °C, 405 °C, and 504 °C.

2.4. Characterization techniques

2.4.1. X-ray diffraction

Crystal structure and lattice parameters were studied using X-ray diffraction technique in the grazing incidence mode. Grazing Incidence X-Ray Diffraction (GIXRD) has been achieved with a PHILIPS X'Pert device with CuKα radiation (wavelength of 1.54 Å) with 4×4 mm^2 cross section parallel incident X-ray beam, by adjusting two Soller slits, and with an angular diffraction detector variation of 0.03° every step with accumulating time of 1 s. The diffraction 2θ angle was measured between 30° and 70° using a detector of scintillation with parallel plates to collimate the diffracted beam. The used X-ray beam angles of incidence in our experiments were 2° and 10°. Considering the X-ray energy corresponding to the wavelength used (~8 keV), the mass attenuation coefficient for Fe ($\mu = 2480$ cm^{-1}), and an intensity attenuation appreciation limit of 1%, the estimated thicknesses of the X-ray observed layer for the 2° and 10° incidence angles used resulted approximately 0.6 μm and 3 μm, respectively. The use of the mass attenuation for Fe is justified because the AISI 316L SS has ~70% of Fe and ~17% Cr in their composition, with only ~10% of Ni.

2.4.2. FIB/SEM analyses

The surface layer structure has been investigated through FIB/SEM. Focused Ion Beam (FIB) has been achieved with a FEI Helios NanoLab ™ 600 (Dualbeam) device which has Ga^+ beam. This ionic beam can erode the surface and make a crater of controlled dimensions [28] making it possible to analyze the sample's cross section. On FIB images the degree of gray is originated by the efficiency of secondary electrons, which will depend on the depth where the ion interacts with the atom of the crystal [29]. This device can switch to the SEM mode by primary electron emission. FIB images could be obtained at 30 kV and ~10 pA, and SEM images need a voltage between 2 kV and 5 kV. Sample can be tilted until 52° to observe surface and cross section in the same run. Possible magnification can be between 2500× and 350,000×.

2.4.3. Optical microscopy

Some surface analyses were done using optical microscopy. That kind of characterization was obtained with an OLYMPUS MG microscope. Surface inspection can be done at a magnification of 500×.

2.5. Sample's preparation

Samples were obtained from a 20 mm diameter AISI 316L SS bar (C: 0.030, P: 0.040, S: 0.026, Si: 0.319, Mn: 1.344, Cr: 17.018, Ni: 10.659, Mo: 2.184, Ti: 0.004, Cu: 0.0380, Fe: balance) by transversally cutting pieces 6 mm thick. Finally, the sample surfaces were polished until mirror appearance. Polishing process ended with a lathe with an emulsion containing 1 μm alumina powder in suspension. Average roughness measured with a Surface Roughness Tester TR200 gives a value of ~40 nm. Before the carburizing (nitriding) process, surfaces were cleaned with alcohol and acetone, and dried in hot air.

3. Results

3.1. Expanded austenite developed under ion carburizing and ion nitriding

Ion nitriding and ion carburizing working parameters used in our experiments are indicated in Table 1. We can see that working pressure was ~5 mbar in all experiments and temperature was between 400 °C and 410 °C, temperatures low enough avoiding precipitation processes. Also, voltages used were according to previous publications by the authors [10,30].

Average roughness of ion nitrided and ion carburized samples was ~130 nm.

On the other hand, current density used was 1.55 mA/cm^2 for nitriding and 2.08 mA/cm^2 for carburizing. Such values assure that there is no precipitation of carbides or nitrides.

Samples were characterized by GIXRD and it was possible to see the three main peaks associated to an fcc structure, equivalent to the austenite of the base material, but with the diffraction peaks (111), (200), and (202) located at lower angles (see Table 2), associated to the EA, provoked by internal strains caused by the entrance of carbon or nitrogen on the interstitial sites of the fcc crystal structure.

At the same time, the analyses of the images of the sample surfaces (Fig. 3) have shown grain borders and slip bands, which can be attributed to internal strains due to the diffusion of nitrogen or carbon into the austenite, and their lodging in interstitial sites, presumably in octahedral ones. Indeed, this statement has been confirmed elsewhere through prediction of lattice parameter expansion with temperature and carbon concentration [31], confirming that EA has been developed on the surface.

In consequence, we have samples of AISI 316L SS with EA developed on their surfaces, obtained by ion nitriding and ion carburizing, whose stability will be studied under high temperature and under the incidence of pulsed high energy light ion beams.

Table 1
Nitriding and carburizing experimental parameters with plasma glow DC discharge at low pressure controlled atmosphere.

Sample	Pressure (mbar)	Voltage (V)	Intensity (A)	Temperature (°C)
Nitriding	4.985	762	0.412	406
Carburizing	5.012	564	0.553	403

Table 2
2θ angular position of (111), (200), and (202) X-ray diffraction peaks of AISI 316L austenitic, ion nitrided and ion carburized steels. Incidence beam has a tilt of 10°.

Planes	AISI 316L SS	Ion nitrided steel	Ion carburized steel
(111)	43.5631	41.0677	42.4162
(200)	50.6104	45.8088	49.1036
(202)	74.5949	68.3143	72.4527

3.2. Heat treatment of expanded austenite

The X-ray diffraction analyses of samples have shown a common behavior for the peaks corresponding to the fcc crystal structure both for austenite and for the resulting expanded austenite. Taking into account such a behavior we will concentrate our studies on the most intense one, i.e. (111).

Specifically carburized AISI 316L SS has been studied at various temperatures and times by GIXRD technique, whose results are shown in Fig. 4. Black line denotes base material; red line expanded austenite without heat treatment; dark blue line 20 hour treatment at 225 °C; green line 40 h at 225 °C; magenta line 20 h at 325 °C; light brown 20 h at 405 °C; indigo line 40 h at 405 °C; dark brown line 60 h at 405 °C, and olive green 20 h at 504 °C.

EA by carburizing without heat treatment has a lattice parameter of 3.6880 Å, which is 2.90% of relative expansion referring base material. In Table 3 this value and the other corresponding to the ones after heat treatments are displayed. By comparing, it is possible to see that heat treatments at 225 °C do not produce any meaningful shifting of (111) peak, which means that at this temperature there is no carbon diffusion from the EA layer [32]. Meanwhile, at 325 °C a small shift to higher angular values, i.e. lower lattice parameter, can be observed. This lattice parameter reduction can be attributed to carbon atoms leaving interstitial sites but in small amounts, because they do not have enough energy to promote massive diffusion. Finally, at 405 °C and 504 °C it is possible to see high shifting attributed to massive loss of C atoms through diffusion, leaving interstitial holes empty.

Similar experiences have been done on the EA developed on AISI 316L by ion nitriding. Fig. 5a shows the different GIXRD (111) 2θ peak positions corresponding to heat treatments equivalent to the ones described before for ion carburizing case. Without thermal treatment, EA by nitriding lattice parameter is 3.8036 Å, corresponding to a 6.13% of relative expansion. In Table 4 all lattice parameter values from samples submitted to thermal processes and their relative

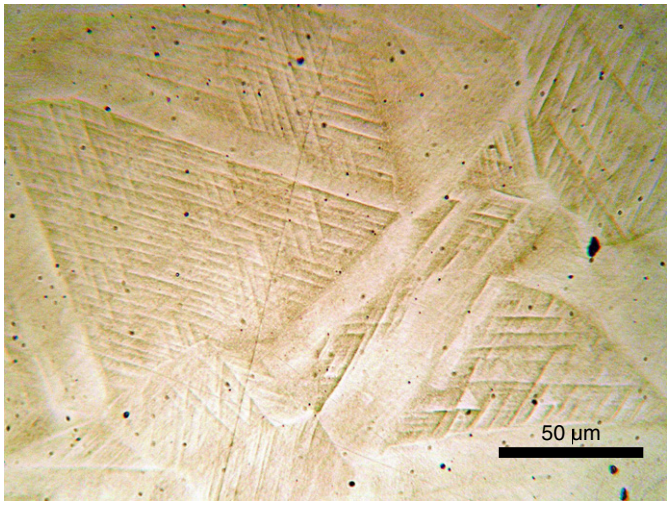

Fig. 3. Optical microscopy of carburized sample. Slip lines can be observed inside the individual grains.

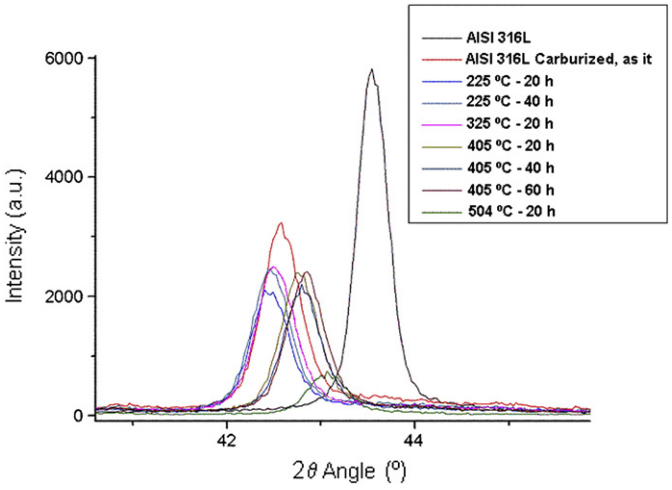

Fig. 4. GIXRD diffractogram at 10° of incidence showing degradation of the crystalline structure of carburized AISI 316L stainless steel confirmed by the shift of (111) peak revealing that lattice parameter diminishes.

expansion can be seen. Apparently, processing time is not so important in view of the negligible low diffraction peak shifting when samples are heat treated at constant temperature for long periods of times. As for carburizing case, heat treatments at 225 °C and 325 °C do not reflect a relevant level of lattice parameter contraction [32], while there is a high lattice parameter reduction when temperature of heat treatment reaches 405 °C and 504 °C. Drawing preliminary conclusions, we can see that the temperature at which ion carburizing and nitriding were performed (~400 °C) is at the same time a threshold for triggering the degradation of the EA structure by diffusion processes. The low intensity of the peak at 504 °C provides us with a clear insight of the EA final degradation. In Fig. 5b it is possible to see the (200) diffraction peak shifting to 2θ higher values with temperature, showing an equivalent behavior to (111).

Nevertheless, for nitriding case while the temperature values induce diffraction peak shifting, at determined fix temperature there was observed a peak intensity reduction tendency which increases with time duration at the considered temperature, without any apparent 2θ angular value variation. This behavior can be appreciated in Fig. 5a for (111) diffraction peak at 405 °C successively showing intensity reduction for 20, 40 and 60 h of treatment respectively. The effect of heat treatment on EA has also been studied elsewhere [30].

On the other hand, to explore the oxidation effect on surface samples after thermal treatment, several ion carburized and nitrided samples have been coated with AlN thin films using reactive sputter magnetron technique [33], before being introduced in the furnace. GIXRD analyses of samples covered with AlN thin films have shown that there is no crystalline structure associated to this compound, i.e. it has an amorphous structure. Indeed, the absence of diffraction peaks corresponding to AlN, facilitates the studies of the 2θ position modification of diffraction peaks corresponding to the EA after

Table 3
List of lattice parameters and relative expansion of the carburized austenite submitted at different temperatures during long lapses of time.

Temperature (°C)	Time (h)	Lattice parameter (Å)	Expansion (%)
225	20	3.6858	2.84
225	40	3.6841	2.79
325	20	3.6800	2.68
405	20	3.6594	2.10
405	40	3.6531	1.93
405	60	3.6521	1.90
504	20	3.6318	1.33

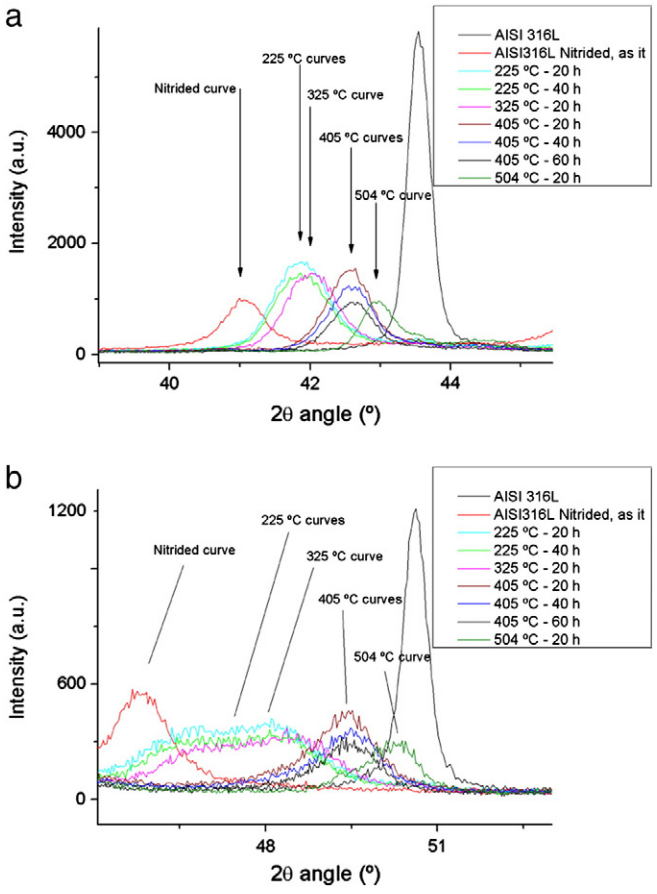

Fig. 5. a) GIXRD diffractogram at 10° of incidence revealing the lowering of the nitrided AISI 316L stainless steel lattice parameter (shown by (111) diffraction peak shifting to higher 2θ angles) with increasing temperature. b) GIXRD diffractogram revealing (200) diffraction peak shifting. There is a threshold at 400 °C when greater temperatures degrade the structure.

heating. The influence of the AlN layer can be inferred by comparing (Fig. 6) diffraction peaks for carburized samples treated during 60 h at 405 °C, with (black line) and without (red line) AlN thin film deposited. EA peaks did not show any differences between surface with AlN and without it, but there is a difference in the peaks located at $2\theta = 33.01°$ and 35.46°, attributed to an α–Fe_2O_3 phase. These results show that while AlN does not affect the EA behavior under the thermal treatment, its presence on the surface works as protection against oxidation during atmospheric heating processes [34].

3.3. Pulsed ion beam irradiation

On this point we will analyze the characterization of the surface of samples on which EA has been developed by ion nitriding and ion carburizing, and have been irradiated with 1, 5, 10 and 20 pulses of high energy light ion beams. The nature of ions has been deuterium

Table 4
Nitrided AISI 316L submitted to high temperature-long time treatments in a furnace at normal atmosphere. Lattice parameter and relative expansion are consigned.

Temperature (°C)	Time (h)	Lattice parameter (Å)	Expansion (%)
225	20	3.7308	4.10
225	40	3.7294	4.06
325	20	3.7173	3.72
405	20	3.6801	2.68
405	40	3.6756	2.56
405	60	3.6710	2.43
504	20	3.6398	1.56

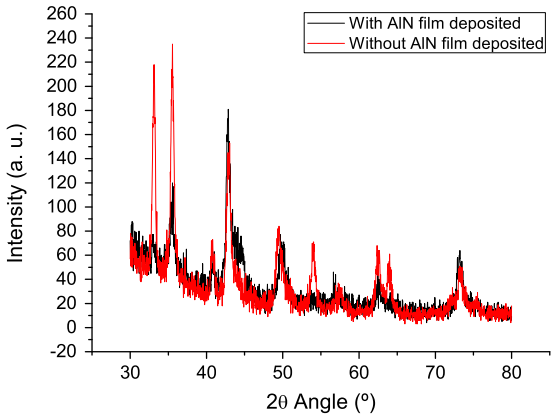

Fig. 6. GIXRD diffractogram at 2° of incidence. Red line identifies AISI 316L carburized treated at 405 °C and 60 h. Black line identifies AISI 316L carburized steel with a AlN film deposited on the surface. Oxides are prevented (see text).

and helium. Once irradiated, the surfaces have been studied using optical microscopy, GIXRD and FIB/SEM.

Optical microscope analyses reveal the morphology of the surface after being irradiated, without cleaning [30]. The morphology of surfaces of EA generated by ion nitriding or by ion carburizing and after being irradiated with one and ten ion beams pulses, either deuterium or helium, has shown significant differences.

In Figs. 7 and 8 typical images of surfaces are shown. It is possible to see slip bands crossover associated to the high thermal gradient involved in the fast heating and cooling processes due to the short duration pulses, provoking residual strains and inducing slip band formation inside the grains [10]. Moreover, some craters of different sizes can be observed overlapping with the general feature. These small craters are typical phenomena related to the pulsed beams accelerated in plasma focus experiments [27], and can be associated to energetic ion clusters present in the beam, also observed in the electron beams accelerated at the same time during the pinch, but in the opposite direction, i.e. backwards [23].

Nevertheless, the damage on the surface depends on the number of incident ion beam pulses. Indeed, in Fig. 8 we can see in ion nitrided sample the accumulative effect of 1 and 10 pulses through the image of a melted surface layer. Observing peeling, severe cracking and melting in ion nitrided steels, we could determine, at first glance, that ion nitriding does not have much resistance to bombardment in comparison to ion carburized ones, at least in surface effects.

GIXRD has been successfully used in other works to analyze the crystalline structure of surface modified by plasma focus discharges [35].

The original crystalline structure of the EA has been modified through pulsed ion beams accelerated with plasma focus, observing that the degree of modification depends on the number of pulses, i.e. 1, 5, 10 and 20 in our experiments. We have concentrated the analyses on the (111) diffraction peak because even though the others, (200) and (202), have shown similar behavior, this is the most intense. Fig. 9 shows the EA on AISI 316L carburized and nitrided under deuterium bombardment. In the figure, black lines identify diffractograms of base material, light blue line the EA before irradiation for both cases, and red, green and dark blue lines the EA after being irradiated with one, five and ten ion beam pulses, respectively.

The results after deuterium ion beam irradiation for both situations, i.e. EA developed by nitriding or carburizing, show that (111) peaks are shifted at greater 2θ diffraction angles, which means a lattice parameter reduction, tending to the original position of austenitic structure of the original AISI 316L SS used. This effect can be explained through the gradual loss of the expansive elements

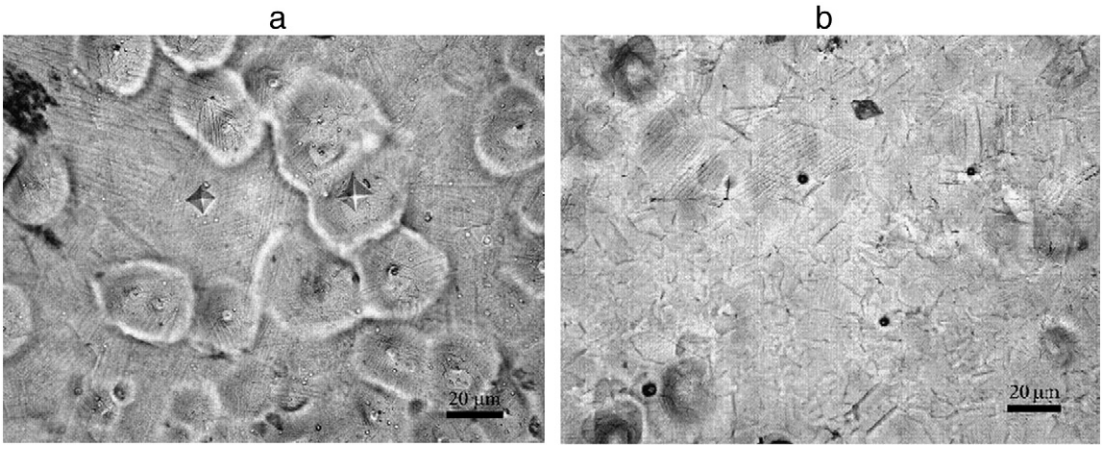

Fig. 7. Images of carburized steel submitted at ion bombardment with optical microscopy at 500×. a) One shot of deuterium, b) ten shots of helium.

(N or C) after each pulse [31]. Thus, ionic pulses work relieving the residual strains [36] that exist in the structure. More precisely, thermal shock effect originated during the ion beam pulse interaction with surface causes a strong surface layer modification of residual stresses, whose effect is accentuated with the number of accumulated ion beam pulses. This gradient was observed elsewhere [37] using Ar and N ion beams also generated in plasma focus discharges on AISI 304 SS, resulting in a growing tensile residual stress with the number of accumulated ion beam pulses. They have observed that while the non-irradiated samples had a superficial residual stress of ~−800 MPa (tensile stress), after one ion beam pulse of Ar ions the residual stress shifted to ~150 MPa–300 MPa (compression stress). Nevertheless, while the (111) diffraction peaks gradually shift to greater diffraction angles, a new one anchored in position 43.3° appears. Indeed, experiments with 20 pulses show that the gradual (111) peak shifting reaches the same $2\theta = 43.3°$ as a limit corresponding to a lattice parameter of 3.6163 Å which, with regard to the lattice parameter normal value of 3.584 Å for austenite, represents an expansion of about 0.90%. On the other hand, this value coincides with the expansion of austenite found in other experiments in which AISI 316L SS was directly irradiated with pulsed ion beams of nitrogen from plasma focus discharges [27].

In Fig. 10 we present the diffractograms corresponding to similar experiments but using He ion beams. The shifting (111) peak behavior is the same as the one in Fig. 9: at increasing number of ion beam pulse irradiation, the 2θ corresponding to the (111) peak is gradually shifted to larger values until the same $2\theta = 43.3°$ limit is reached. Nevertheless, while for nitrided samples, and overlapped with (111) gradual peak expansion, in all cases the peak appears exactly at $2\theta = 43.3°$; such incipient peak is not present on the sequence of diffractograms for carburized case.

By combining FIB and SEM techniques, it is possible to study the surface morphology [28] with more precision [38]. FIB uses a beam of Ga^+ to penetrate the surface and detect secondary electrons from the affected layer [39]. SEM images are obtained when the device uses primary electrons in the bombardment [40] instead of gallium ions. FIB images of the top of surfaces are presented in Fig. 11. During deuterium and helium ion beam irradiation of EA, both types of ions cause material ejection [41], leaving a surface damage as seen in the mentioned figure.

On the other hand, cross-sectional images can also be analyzed with FIB technique (Fig. 12). The irradiation of EA developed under carburization presents two behaviors: carburized sample under one He pulse has no amorphous film in the very surface and there are sharp grain borders. Inside the grains a kind of peeling can be seen, probably caused by residual strain release [42] during the sample cutting with Ga^+ bombardment, considering that EA has compressive strains. On top of sample's surface carburized with five deuterium pulses, we can see an irregular structure with bubbles caused by fast cooling and the formation of amorphous layer (with the thinnest zone of 1.26 μm). This malleable zone is responsible for the not perfect definition of craters. There is a bunch of little grains at ~3 μm deep that can be seen with more definition on the same region snapshot in Fig. 13.

These crystallites have sizes ranging between 35.6 and 217.8 nm with some crystallite cluster development. At first glance crystallites

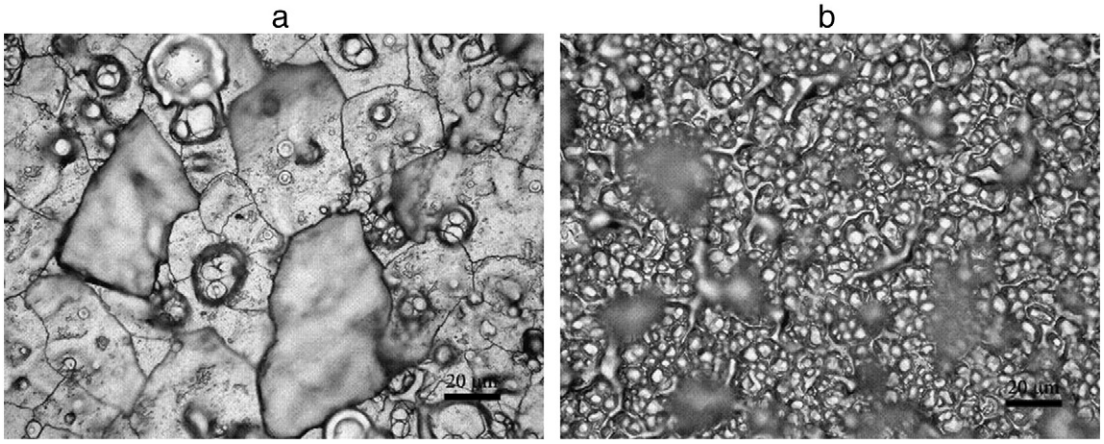

Fig. 8. Nitrided stainless steel surface analyzed using optical microscopy. a) One shot of deuterium, b) ten shots of helium.

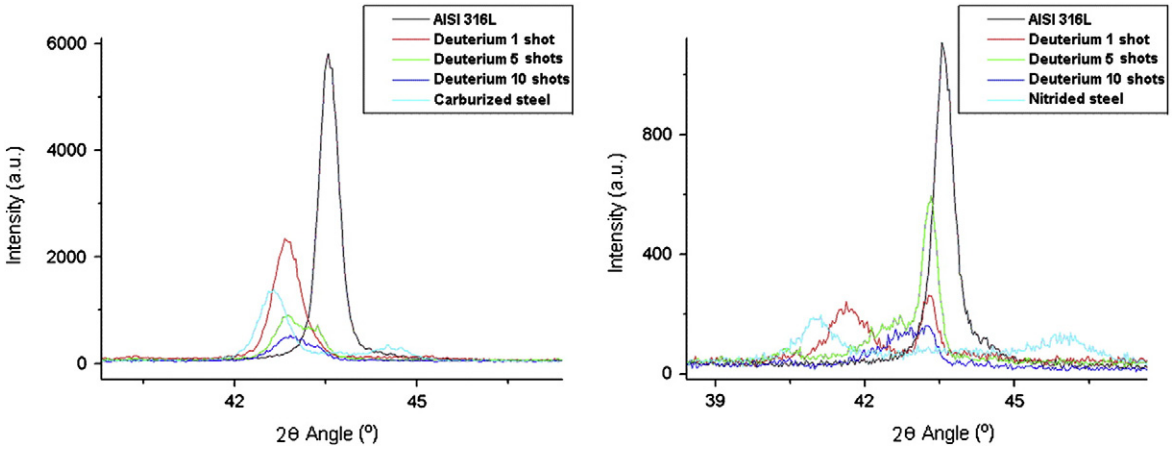

Fig. 9. GIXRD diffractograms taken at 10° (left image) and 2° (right image). Left image represents expanded austenite by carburizing bombarded with deuterium. Right one is expanded austenite by nitriding bombarded with deuterium.

could be explained as centers of crystalline structure nucleation with very light coarsening, halted immediately by the quick drop of temperature after melting.

In the sample cross-section nitrided with five deuterium pulses, Fig. 12 part c, a huge bubble (~1.61 μm diameter) immersed in an amorphous ~3 μm thick layer can be seen, proving that the induced thermal shock by the intense bombardment provoked steel melting. We can describe this bubble as a crater developed during the incidence of one ion beam pulse, and covered by the melted material during subsequent beam incidence. Besides, in this case, at depths of 3 μm there exists an irregular layer (thickness varying between 0.59 μm and 1.27 μm) formed by crystallites. The presence of crystallites can be seen down to the same depth as observed for the carburized with five deuterium pulse sample's case. This behavior can be described by the high temperatures involved at the topmost surface, melting the first nanometers [35] and initialization of diffusion processes. These processes only work in a thickness of 3 μm during a few hundreds of nanoseconds. There is a crack whose depth is about 7 μm.

4. Discussion

By comparing the morphological structures observed on FIB/SEM scans of Fig. 12 with the diffractograms we can correlate the presence of crystallites down ~3 μm deep with the stable X-ray diffraction peaks at ~43.3°. Indeed, we have systematically observed the presence of this dark structures down the surface for each experimental situation in which the $2\theta = 43.3°$ are present. The peak position shows a small expansion of the normal lattice parameter of austenite. This can be explained considering that the crystallites are small crystals of austenite, slightly expanded, that began to grow partially in the melted material after the ion beam incidence.

Ion impact induces disorder in the structure and faults in the crystal lattice [43]. N or C from the EA is missed due to diffusion, with the additional melting down of the surface layer due to the thermal shock provoked by the collective effect associated to the high fluence of ions in each beam [27]. When the temperature drops, steel rearranges its atoms and starts nucleation processes [44], but this quick process stops immediately giving rise to crystallites of nanometric sizes, as can be seen in Fig. 13. These crystallites have a high residual strain [45] induced by the resulting tensile stress of the irradiated superficial layers [37], and their lattice parameter becomes fixed at ~3.6163 Å, which correspond to the X-ray diffraction peak at $2\theta = 43.3°$.

Most of the neighborhood presents the uniform structure attributable to a partially amorphous bulk. Those small crystals turned out to be tensioned by the matrix in which they are included, inducing the little expansion of the austenite, whose observed constant of expansion could be related to the equilibrium forces between the crystal expansion and the limit of traction that the amorphous bulk can support. This could be compatible with the fact that the observed phenomena do not depend on the number of pulsed ion beam used.

The peak position at $2\theta = 43.3°$ proves to be independent of the nature of the origin of the EA, i.e. developed by ion nitriding or

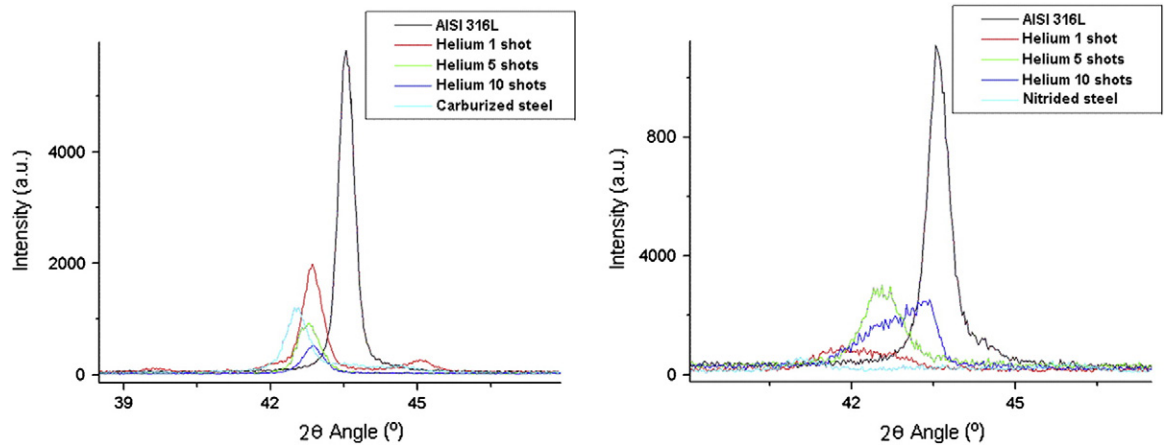

Fig. 10. GIXRD diffractograms. Left image is measured at 10° of incidence and represents carburized steel submitted to helium bombardment. The right one is measured at 2° of incidence, and is the analysis of nitrided steel with 0, 1, 5, and 10 helium shots.

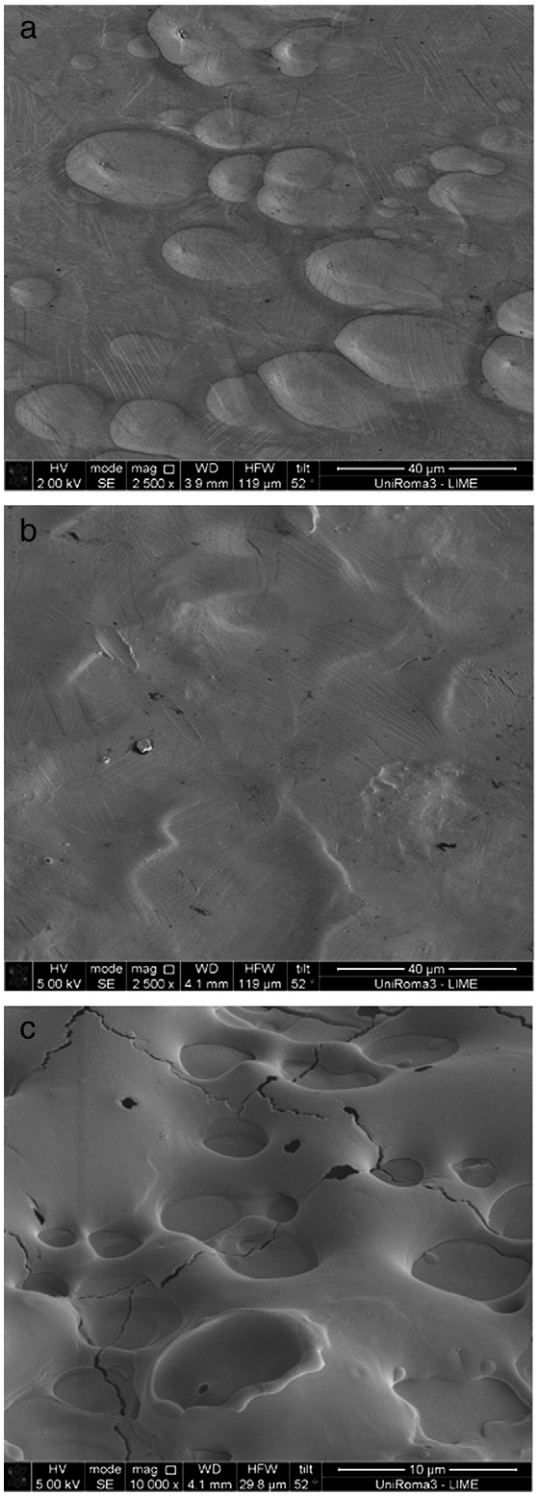

Fig. 11. Surface FIB/SEM images. a) Carburized steel and one shot of helium, b) carburized steel and five shots of deuterium, c) nitrided steel and five shots of deuterium.

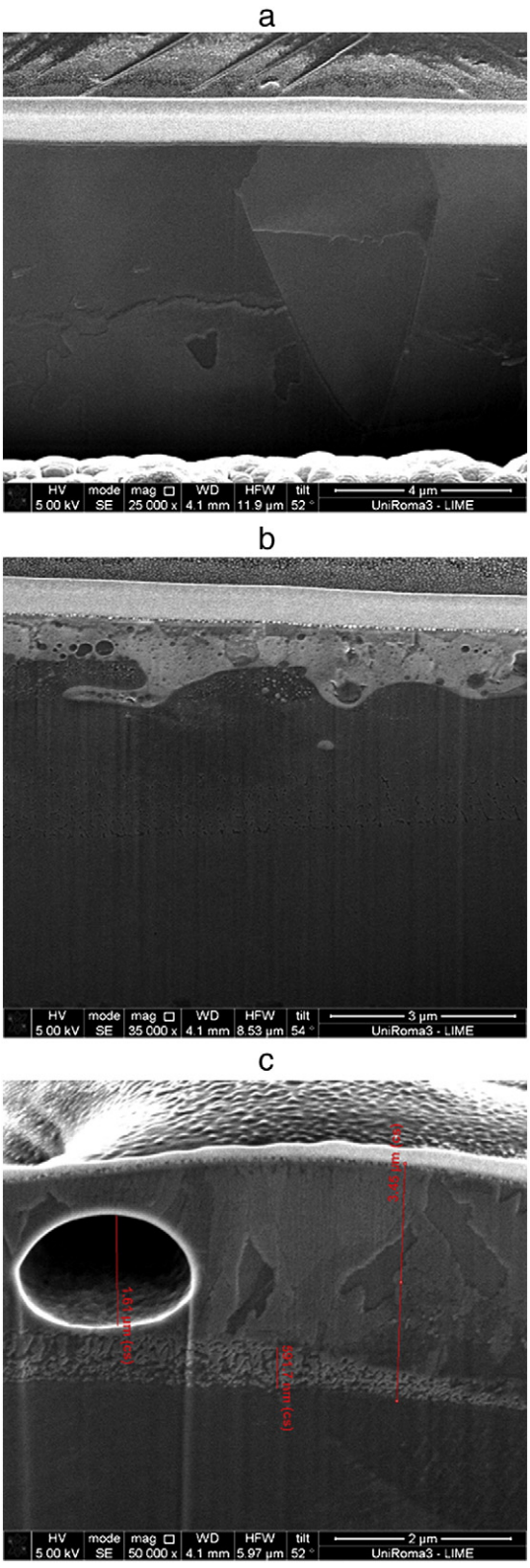

Fig. 12. Cross-sectional FIB/SEM images, a) carburized steel and one shot of helium, b) carburized steel and five shots of deuterium, c) nitrided steel and five shots of deuterium.

ion carburizing, and independent of the nature of ions (deuterium or helium) used on the pulsed ion beams, compatible with the idea that EA can be considered as a crystalline structure without important amounts of N or C in their structure.

In addition to the closeness to the surface layer effect described above, below the first ~3 µm, another less intense thermal effect takes place. As it is farther from the surface, where the ions interact directly with the atoms of the EA layer, thermal effect turns out to be attenuated giving rise to a different process. Indeed, a gradual contraction of the EA with the number of pulsed ion beam incidents was observed through diffractograms. We can consider that this lattice contraction is due to the gradual loss of N or C from the lattice matrix during each pulse. In spite of the fact that the temperature after the incidence becomes well above the 300 °C [32], the short duration of pulses allows also fast cooling down through heat

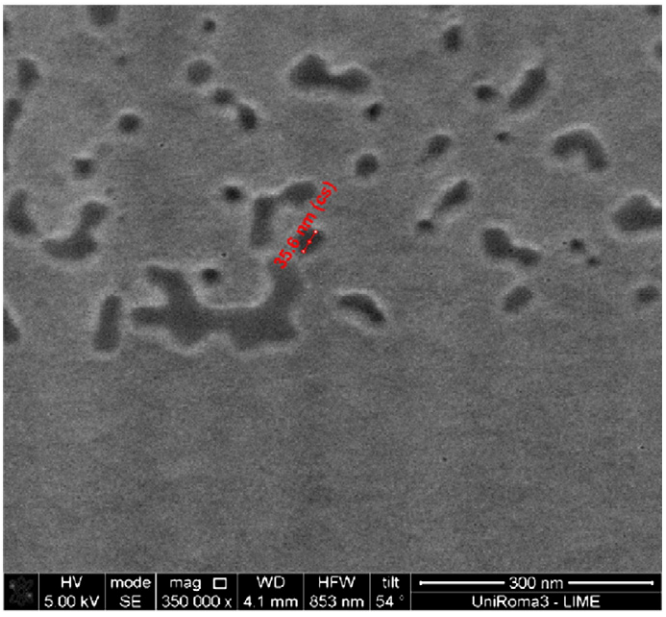

Fig. 13. FIB/SEM image from cross-section of carburized sample irradiated with five deuterium pulses. Grain zone is detailed showing the crystallites and clusters of them localized at 3 μm deep. These crystallites are formed, presumably, by austenite at high residual stresses.

conduction to the sample bulk [46,47]. This process conduces to the partial loss of N [48] and C from the lattices gradually reducing the lattice parameter after each incident ion beam pulse, and occupying deeper interstitial holes [32]. Nevertheless, it was observed that this contraction tends to move towards the diffraction peak at $2\theta = 43.3°$, i.e. a little higher than the diffraction peak of non perturbed austenite.

Finally, the results associated to heat treatments in furnace at normal atmosphere have shown that below 400 °C, independent of the time duration of the treatment, the EA is stable. Nevertheless, over this temperature, EA is rapidly degraded returning to the original state of austenite, characteristic in our case of the AISI 316L SS used. Nevertheless, we did not find the presence of the diffraction peak at $2\theta = 43.3°$ found during pulsed ion beam irradiation. It is necessary to point out that the 400 °C limit temperature coincides with the temperature at which the process of EA development takes place during ion nitriding or carburizing.

5. Conclusions

The stability of EA under high temperature (in a furnace at normal atmosphere) and under irradiation with high energy, high fluence rate pulsed light ion beams, has been studied. The EA has been generated by ion nitriding and ion carburizing at a pressure of 5 mbar and processing temperature of 400 °C of AISI 316L stainless steel, without any nitride or carbide precipitates formation. The results can be summarized as follows:

- Except for the difference of lattice parameters of EA originated by ion nitriding or ion carburizing (3.8036 Å and 3.6880 Å respectively), the results obtained in our research are qualitatively equivalent for both situations.
- Heat treatment in a furnace at normal atmosphere has shown that the EA lattice parameter (observed as 2θ diffraction peak values) has resulted virtually unmodified for temperatures below 325 °C.
- Over 325 °C and up to 504 °C (maximum experienced temperature), EA lattice parameter results gradually reduced with increasing temperature (because of diffusion thermal activation), remaining unchanged with lasting time at every prefixed temperature. Nevertheless, there is a tendency to a diffraction peak intensity reduction with increasing lasting time for every fixed temperature.
- Superficial layers result in oxidation during the thermal treatment. Nevertheless, the EA behavior with temperature was no influenced by oxidation process.
- Under ion irradiation with ion beam pulses EA is degraded by the accumulation of pulses because of diffusional mechanisms activated by the induced fast temperature increasing.
- Image cross section of surface layers has shown two separate layers. A layer of ~3 μm closer to the surface, followed by a less perturbed deeper one. Considering the maximum range of energetic ions (~2.43 μm), we can attribute this first superficial layer to the direct interaction of ions with atoms of the lattice, while below these first ~3 μm a secondary thermal effect by thermal conduction takes place.
- The layer closer to the surface melted (~3 μm), thus developing a more amorphous matrix due to the high fluence rate of the energetic ion beams arriving at the surface.
- At depths of ~3 μm small crystallites are formed, attributable to austenite recrystallization during the fast cooling down process followed after ion beam pulse incidence, with a lattice calculated parameter of 3.6163 Å.
- Through X-ray diffraction it was possible to see that the lattice parameter of EA was gradually reduced after the incidence of every ion beam pulse tending to move towards to the lattice parameter of 3.6163 Å, i.e. to austenite with a small expansion of ~0.90%. This slightly expanded situation of austenite can be attributable to the tensile residual stress induced on small crystals by the fast cooling effect.

In spite of the fact that EA is not the case, we can say that pulsed ion beams generated in plasma focus discharges can be considered as a useful tool to test materials that can be used in problems like nuclear technology, more specifically in first wall problems associated to nuclear fusion.

Acknowledgments

We are grateful to Daniele de Felicis and Javier Cruceño for their dedication to the development of several of the characterization techniques used. Research work granted through PICT 2008-0374 of ANPCyT, and Project IT/10/06 of the "Programa de Cooperación Bilateral Científico-Tecnológico Argentino-Italiano MINCYT-MAE".

References

[1] H.K. Lo, C.H. Shek, J.K.L. Lai, Mater. Sci. Eng. R 65 (2009) 39.
[2] A. Matthews, A. Leyland, B. Dorn, P.R. Stevenson, M. Bin-Sudin, C. Rebholz, A. Voevodin, J. Schneider, J. Vac. Sci. Technol. A 13 (3) (1995) 1202.
[3] A. Leyland, D.B. Lewis, P.R. Stevenson, A. Matthews, Surf. Coat. Technol. 62 (1993) 608.
[4] A. Matthews, A. Leyland, Surf. Coat. Technol. 71 (1995) 88.
[5] Y. Sun, J. Mater. Proc. Technol. 168 (2005) 189.
[6] E. Menthe, K.-T. Rie, Surf. Coat. Technol. 116–119 (1999) 199.
[7] M.P. Fewell, J.M. Priest, M.J. Baldwin, G.A. Collins, K.T. Short, Surf. Coat. Technol. 131 (2000) 284.
[8] T. Christiansen, M.A.J. Somers, Scr. Mater. 50 (2004) 35.
[9] J. Feugeas, B. Gómez, A. Craievich, Surf. Coat. Technol. 154 (2002) 167.
[10] J. García Molleja, L. Nosei, J. Ferrón, E. Bemporad, J. Lesage, D. Chicot, J. Feugeas, Surf. Coat. Technol. 204 (2010) 3750.
[11] G. Amarendra, B.K. Panigrahi, S. Abhaya, C. David, R. Rajaraman, K.G.M. Nair, C.S. Sundar, B. Raj, Appl. Surf. Sci. 255 (2008) 139.
[12] H.M. Chung, "Assessment of Void Swelling in Austenitic Stainless Steel Core Internal", Argonne National Laboratory, Report NUREG/CR-6897 ANL-04/28 Prepared for Division of Engineering Technology Office of Nuclear Regulatory Research, U.S. Nuclear Regulatory Commission, Washington DC, USA, January 2006.
[13] US Department of Energy, Office of Fusion Energy Sciences, Final Report, 2009, (http://burningplasma.org/renew.html).
[14] E.I. Moses, Nucl. Fusion 49 (2009) 104022(9 pp.).
[15] S.E. Bodner, D.G. Colombant, J.H. Gardner, R.H. Lehmberg, S.P. Obenschain, L. Phillips, A.J. Schmitt, J.D. Sethian, R.L. McCrory, W. Seka, C.P. Verdon, J.P. Knauer, B.B. Afeyan, H.T. Powell, Phys. Plasmas 5 (1998) 1901.
[16] C.X. Li, T. Bell, Wear 256 (2004) 1144.
[17] S. Corujeira Gallo, H. Dong, Vacuum 84 (2010) 321.
[18] J.W. Mather, Phys. Fluids 7 (1964) S28.
[19] M. Milanese, R. Moroso, J. Pouzo, IEEE Trans. Plasma Sci. 21 (1993) 373.

[20] L. Rico, B.J. Gómez, J. Feugeas, O. de Sanctis, Appl. Surf. Sci. 254 (2007) 193.
[21] T. Haruki, H. Reza Yousefi, K. Masugata, J.-I. Sakai, Y. Mizuguchi, N. Makino, H. Ito, Phys. Plasmas 13 (2006) 082106.
[22] T. Hussain, R. Ahmad, I.A. Khan, J. Siddiqui, N. Khalid, A. Saleem Bhatti, S. Naseem, Nucl. Instrum. Methods Phys. Res. B 267 (2009) 768.
[23] V. Nardi, W. Bostick, J. Feugeas, W. Prior, Phys. Rev. A 22 (1980) 2211.
[24] M.M. Milanese, R.L. Moroso, IEEE Trans. Plasma Sci. 33 (5) (October 2005).
[25] R.L. Klueh, D.S. Gelles, S. Jitsukawa, A. Kimura, G.R. Odette, B. van der Schaaf, M. Victoria, J. Nucl. Mater. 307–311 (2002) 455.
[26] G. Sánchez, G. Grigioni, J. Feugeas, Surf. Coat. Technol. 70 (1995) 181.
[27] J. Feugeas, L. Rico, L. Nosei, B. Gómez, E. Bemporad, J. Lesage, J. Ferrón, Surf. Coat. Technol. 204 (2010) 1193.
[28] X. Song, K.B. Yeap, J. Zhu, J. Belnoue, M. Sebastiani, E. Bemporad, K.Y. Zeng, A.M. Korsunsky, Procedia Eng. 10 (2011) 2190.
[29] E. Bemporad, M. Sebastiani, F. Casadei, F. Carassiti, Surf. Coat. Technol. 201 (2007) 7652.
[30] L. Nosei, M. Ávalos, B.J. Gómez, L. Náchez, J. Feugeas, Thin Solid Films 468 (2004) 134.
[31] N.N. Rammo, O.G. Abdulah, J. Alloys Compd. 420 (2006) 117.
[32] B. Sartowska, J. Piekoszewski, L. Waliś, J. Stanisławski, L. Nowicki, R. Ratajczak, M. Kopcewicz, J. Senatorski, Vacuum 81 (2007) 1188.
[33] V. Mortet, A. Vasin, P.-Y. Jouan, O. Elmazria, M.-A. Djouadi, Surf. Coat. Technol. 176 (2003) 88.
[34] C.-Y. Lin, F.-H. Lu, J. Eur. Ceram. Soc. 28 (2008) 691.
[35] G. Murtaza, S.S. Hussain, M. Sadiq, M. Zakaullah, Thin Solid Films 517 (2009) 6777.
[36] A.H. Heuer, F. Ernst, H. Kahn, A. Avishai, G.M. Michal, D.J. Pitchure, R.E. Ricker, Scr. Mater. 56 (2007) 1067.
[37] M.J. Marques, J. Pina, A.M. Dias, J.L. Lebrun, J. Feugeas, Surf. Coat. Technol. 195 (2005) 8.
[38] H. Söderberg, Microstructural characterization and hardening behavior of reactive magnetron sputtered TiN/Si_3N_4 multilayer thin films (grade thesis), Luleå University of Technology, Sweden, 2004.
[39] E. Bemporad, M. Sebastiani, M.H. Staia, E. Puchi Cabrera, Surf. Coat. Technol. 203 (2008) 566.
[40] K. Tokaji, K. Kohyama, M. Akita, Int. J. Fatigue 26 (2004) 543.
[41] M.V. Roshan, R.S. Rawat, A.R. Babazadeh, M. Emami, S.M. Sadat Kiai, R. Verma, J.J. Lin, A.R. Talebitaher, P. Lee, S.V. Springham, Appl. Surf. Sci. 255 (2008) 2461.
[42] K.J. Kim, J. Ginsztler, S.W. Nam, Mater. Lett. 59 (2005) 1439.
[43] B. Chalmers, Metalurgia Física, John Wiley & Sons, Aguilar S.A., 1959.
[44] Y.-M. Chiang, D. Birnie III, W.D. Kingery, Physical Ceramics, Principles for ceramics science and engineering, Ed. Wiley–MIT, 1997.
[45] L. Nosei, S. Farina, M. Ávalos, L. Náchez, B.J. Gómez, J. Feugeas, Thin Solid Films 516 (2008) 1044.
[46] K. Ram Mohan Rao, S. Mukherjee, P.M. Raole, I. Manna, Surf. Coat. Technol. 200 (2005) 2049.
[47] M. Tsujikawa, D. Yoshida, N. Yamauchi, N. Ueda, T. Sone, S. Tanaka, Surf. Coat. Technol. 200 (2005) 507.
[48] D. Manova, S. Mändl, H. Neumann, B. Rauschenbach, Surf. Coat. Technol. 201 (2007) 6686.